Wide-Area Analysis-Ready Radar Backscatter Composites

David Small, *Senior Member, IEEE*, Christoph Rohner, Nuno Miranda, Marius Rüetschi, and Michael E. Schaepman, *Senior Member, IEEE*

***Abstract*— The benefits of composite products are well known to users of data from optical sensors: cloud-cleared composite reflectance or index products are commonly used as an analysis-ready data (ARD) layer. No analogous composite products are currently in widespread use that is based on spaceborne radar satellite backscatter signals. Here, we present a methodology to produce wide-area ARD composite backscatter images. They build on the existing heritage of geometrically and radiometrically terrain corrected level 1 products. By combining backscatter measurements of a single region seen from multiple satellite tracks (incl. ascending and descending), they are able to provide wide-area coverage with low latency. The analysis-ready composite backscatter maps provide flattened backscatter estimates that are geometrically and radiometrically corrected for slope effects. A mask layer annotating the local quality of the composite resolution is introduced. Multiple tracks are combined by weighting each observation by its local resolution, generating seamless wide-area backscatter maps suitable for applications ranging from wet snow monitoring to land cover classification or short-term change detection.**

***Index Terms*— Radar cross sections, radar scattering, radar signatures, radar terrain factors.**

I. Introduction

COMPOSITE products are well-known to users of optical sensors, as it is commonplace to automatically generate cloud-cleared reflectance data. For example, in the case of the well-known MODIS "Moderate Resolution Imaging Spectroradiometer" sensor, if one browses through its product Table [1], [2], one notes that almost all entries are composite products.

Recall that remote sensing products are generally distinguished by processing levels, quoted from [3] (own emphasis):

1) *L0:* Reconstructed unprocessed instrument data at full resolution
2) *L1A:* Reconstructed unprocessed instrument data at full resolution, time referenced, and annotated with ancillary information, including radiometric and geometric calibration coefficients and georeferencing parameters (i.e., platform ephemeris) computed and appended but not applied to the L0 data.
3) *L1B:* L1A data that has been processed to sensor units (i.e., radar backscatter cross section, brightness temperature, etc.). Not all instruments will have an L1B equivalent.
4) *L2:* Derived environmental variables (e.g., ocean wave height, soil moisture, ice concentration) at the same resolution and location as the source data.
5) *L3:* Variables mapped on *uniform space-time scales*, usually with some *completeness and consistency properties* (e.g., missing points interpolated, *complete regions mosaicked together from multiple orbits*).
6) *L4:* Model output or results from analyses of lower-level data (i.e., variables that were not measured by the instruments but instead are derived from these measurements).

In comparison to the MODIS product table, no analogous standardized set of methodologies to generate L3 backscatter products from L1 radar data have been established to date. ESA's Sentinel-1 (S-1) satellites are providing free and open data with unprecedentedly high geolocation quality [4]–[6] and wide spatial coverage at high temporal resolution. In this article, we introduce a new standardized approach for the generation of L3 backscatter composites. This enables multitrack and multisensor integration, opening the door to the "daily" level of temporal resolution that has long been a goal [7].

We begin with a review of L1 terrain corrections in Section II. This is followed in Section III with a description and demonstration of local resolution weighting (LRW) applied to generate L3 backscatter composites. Applications of the backscatter composites are discussed at the end of Section IV. Conclusions and recommendations are then summarized.

II. Level 1 Terrain Corrections

We first review products based on conventional range-Doppler geocoding (i.e., *geometric* terrain correction), and illustrate the benefits of *radiometric* terrain correction (i.e., "RTC" product type [8]), whereby the influence of mountainous terrain on the retrieved radiometry is mitigated.

Manuscript received September 9, 2019; revised September 28, 2020 and December 21, 2020; accepted January 24, 2021. Date of publication February 11, 2021; date of current version December 6, 2021. This work was supported by the ESA-funded Telespazio/Vega IDEAS+ VEGA/AG/15/01757 Project. *(Corresponding author: David Small.)*

David Small, Christoph Rohner, and Michael E. Schaepman are with the Remote Sensing Laboratories, Department of Geography, University of Zurich, 8057 Zurich, Switzerland (e-mail: david.small@geo.uzh.ch).

Nuno Miranda is with the European Space Agency, European Space Research Institute (ESRIN), 00044 Frascati, Italy (e-mail: nuno.miranda@esa.int).

Marius Rüetschi is with the Land Change Science Unit, Swiss Federal Institute for Forest, Snow and Landscape Research WSL, CH-8903 Birmensdorf, Switzerland (e-mail: marius.rueetschi@wsl.ch).

Digital Object Identifier 10.1109/TGRS.2021.3055562

A. Geometric Terrain Correction (GTC)

In many "geocoding" analyses, each synthetic aperture radar (SAR) input product is first individually translated to map geometry as "geometrically terrain corrected" GTC products. Range-Doppler geolocation [9], [10] is typically applied, whereby external precise orbital state vectors (OSVs) are interpolated at each azimuth line. The backscatter values are then resampled from the input products' slant or ground range geometry into the map geometry of the digital elevation model (DEM) being used. "Blind" geocoding with modern sensors is possible, whereby no "tie-points" need to be used [11]. One assumes that an accurate geometric calibration [12] has been applied to the sensor, and that the L1 product annotations can be applied directly. For even higher accuracy (e.g., geodetic applications), further corrections for atmospheric path delay distortions, solid Earth tides, frameshift, and further SAR processor-specific artifacts can be considered during geolocation [5]. Depending on the desired resolution of the output product, these latter corrections may or may not provide added benefit. However good the geometric correction is, only the *positions* of the measurements are adjusted in GTC backscatter products: their backscatter values (σ_E^0 or γ_E^0) themselves remain ellipsoid-based. Methods for radiometric corrections evolved over the years from relatively simple approaches that used the local angle of incidence [13]–[16] to a trend in recent years of acknowledging that "heteromorphic" approaches are required [8], [17]–[19]. These approaches acknowledge the "heteromorphism" [20] (i.e., lack of 1-to-1 correspondence) between the topologies inherent in radar versus map (DEM) geometries.

B. Radiometric Terrain Correction (RTC)

Whereas in the case of GTC products, only the *location* of pixels is modified between the L1 input product and the output map geometry, in the case of RTC products *both the location and the brightness* (radiometry) of each pixel is corrected to account for terrain-induced modulations of the image radiometry. First, an image simulation is performed by proceeding through the available DEM and projecting each DEM triangular facet into the plane perpendicular to the local slant range direction. The areas are summed at each image location (range and azimuth), with facets covered by radar shadow carefully excluded from the summation. The projection into the plane perpendicular to slant range follows the gamma nought convention, and ensures that the actual area seen by the sensor is replicated in the final image simulation [8]. The RTC backscatter (γ_T^0) is computed by sourcing the normalized radar cross section generated during the image simulation to provide the local area, rather than a simple ellipsoid-based incident angle model traditionally widely applied to backscatter (σ_E^0 or γ_E^0) in the literature. Whereas the normalization area $\underline{A}_\gamma(\theta_E)$ is a function of the ellipsoidal incident angle θ_E for γ_E^0 [8]

$$\gamma_E^0 = \frac{A_\beta}{\underline{A}_\gamma(\theta_E)} \cdot \beta^0 = \beta^0 \cdot \tan\theta_E \tag{1}$$

in the case of γ_T^0, the normalization area $A_\gamma(r, a)$ is individual to each range and azimuth coordinate (r, a) in the L1 product

$$\gamma_T^0 = \frac{A_\beta}{A_\gamma(r, a)} \cdot \beta^0. \tag{2}$$

Fig. 1 shows GTC and RTC products of the same data set juxtaposed for comparison. In the top row, GTC vertical-transmit horizontal-receive (VH) backscatter (γ_E^0) is shown for a set of three S-1 Interferometric Wide-swath (IW) Ground Range Detected High-resolution (GRDH) products covering the central Alps acquired on May 4 and 5, 2016. In the lower row, the associated RTC images (γ_T^0) are shown for comparison. Note how the dark wet snow backscatter signals are mixed with terrain-induced brightness distortions in the GTC images in the top row, but are directly visible in the RTC image in the bottom row. Given that RTC backscatter retrievals show less contamination from the effects of terrain, they are a preferred product for higher-level analysis, i.e., they are an "Analysis Ready Data" (ARD) product.

Fig. 2 shows a geocoded version of the ascending image simulation (in map geometry). One can understand the RTC product roughly as a β^0 GTC backscatter image divided by the area (seen in the image simulation). Note how the mountainous foreslopes are much brighter in the area image, while the back-slopes are darker. By dividing the β^0 backscatter by the local contributing area, the foreslopes are proportionally darkened while the back-slopes are lightened in comparison to flat regions.

The algorithm for producing standardized RTC terrain-flattened gamma nought (γ_T^0) was published in [8] and is referenced within the "CARD4L" CEOS ARD for Land specifications [21]. The algorithm's pseudo-code was used as a template while implementing the terrain-flattening module within ESA's SentiNel Application Platform (SNAP) toolbox [22]. Some errors in SNAP's implementation remain [23] and will hopefully be remedied. Further implementations [18], [19] have been widely applied, e.g., at the Alaska Satellite Facility. Issues surrounding standardized RTC production for integration in data cubes were reviewed in [23].

C. Added Value of Radiometric Flattening

Gamma nought backscatter retrieved from three S-1 tracks covering Switzerland is shown in Fig. 3. The green region was covered by one ascending track, while the yellow and purple regions were covered by one ascending track and one descending track each. The gray region was covered by all three tracks (one descending, two ascending). A further ascending track covering the western extreme and another descending track covering the eastern extreme is not shown, as red/green/blue (RGB) overlays can only unambiguously highlight three tracks. Fig. 3(a) shows the GTC gamma nought backscatter γ_E^0, while in Fig. 3(b), the RTC gamma nought γ_T^0 is shown. Note how the mountainous regions produce wildly different backscatter values on the fore- versus backslopes in the GTC overlay, and that the terrain-induced distortions clearly visible in the GTC overlay are strongly reduced in the RTC overlay. It should be

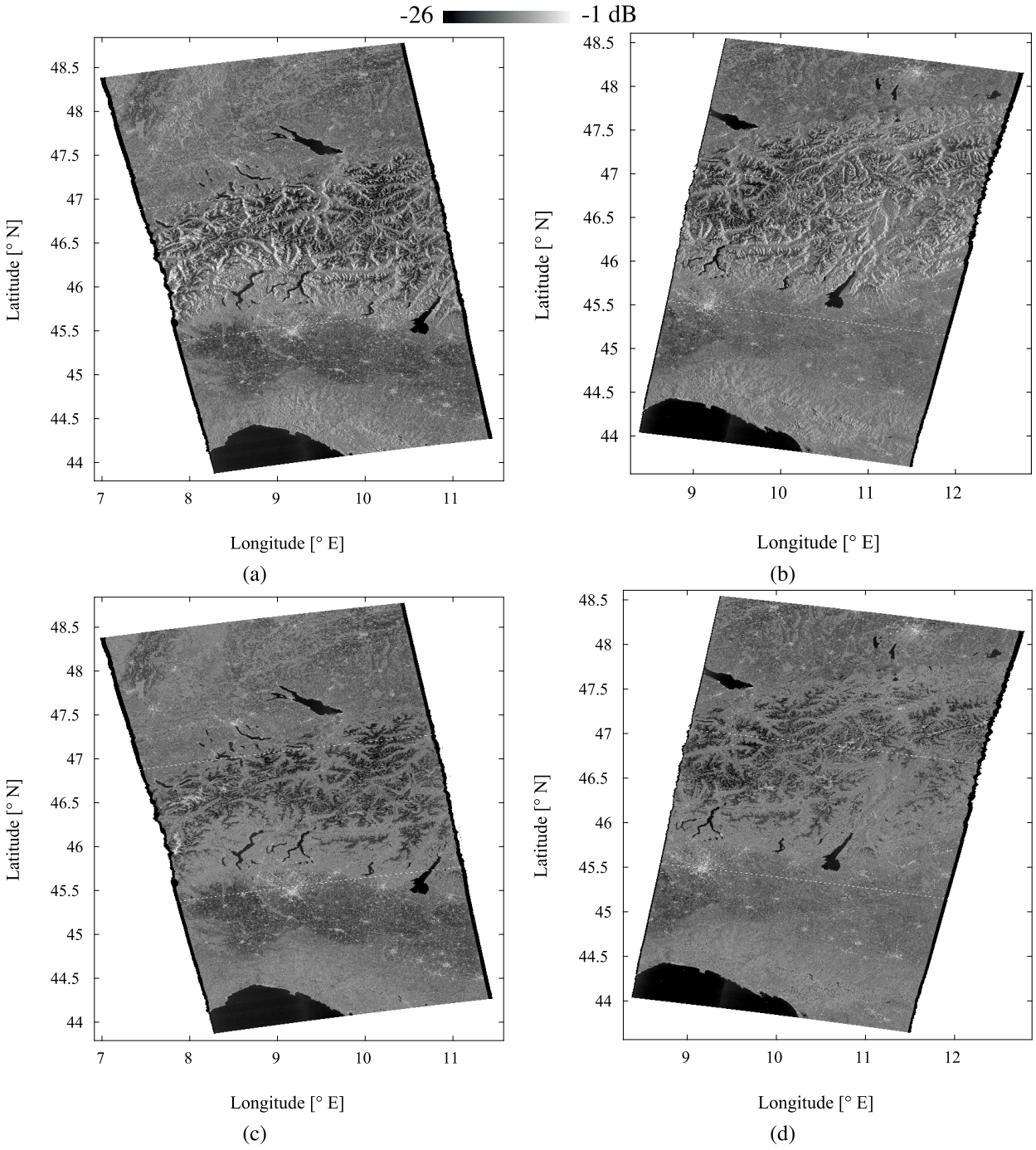

Fig. 1. Sentinel-1 VH-pol. backscatter mosaics of central Alps in of three azimuth-adjacent Interferometric Wideswath (IW) Ground-Range-Detected-HighRes (GRDH) products–geographic coordinates–Shuttle Radar Topography Mission (SRTM) Digital Surface Model (DSM) applied–(a) 2016.05.04 γ^0_E, (b) 2016.05.03 γ^0_E, (c) 2016.05.04 γ^0_T, (d) 2016.05.03 γ^0_T–contains modified Copernicus Sentinel data (2016).

noted that thematic land cover change interpretation would be severely impaired by terrain-induced distortions when the analysis is based on a GTC time series. However, the RTC products allow interpretations also within the mountainous terrain [24].

D. Local Resolution in GTC and RTC Products

Although the improvement to the thematic backscatter estimation is much improved in RTC versus GTC products, the *local resolution* within both product types is identical. The poor local resolution on *foreslopes* in GTC products is made visible by their bright return (see Fig. 1). Although the distortion in the local radar brightness is strongly mitigated in the RTC case, the poor local resolution remains on the foreslopes. Indeed, no further improvement is conceivable given only a single image acquisition, as in that case no better-resolved backscatter values are available at those locations.

In the following, a novel further stage of processing is introduced that works to mitigate that remaining issue.

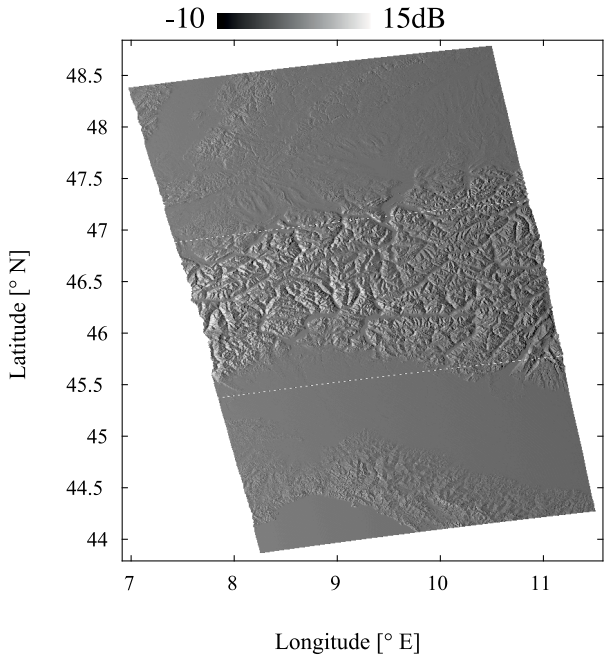

Fig. 2. Local contributing area of three azimuth-adjacent Sentinel-1 IW GRDH products from 2016.05.04-SRTM DEM applied-Central Alps.

III. Backscatter Composites Through LRW

In this section, we introduce a second stage process whereby the highly variable local resolution of radar imagery in mountainous terrain is dealt with by combining multiple data acquisitions acquired from differing geometries. Mosaicking processes typically place backscatter values from a single date next to adjacent areas viewed on a different date, applying Boolean class membership to each input data set. Here, we instead apply the concept of fuzzy class membership [25] to each pixel, with variable (fractional) degrees of attribution from each input set based on the local resolution.

This method can be used to produce wide-area backscatter composites for a variety of applications that maintain validity also in mountainous regions. Unlike "one-off" SAR mosaicking approaches [26]–[30], LRW combines all available data into a local backscatter estimate based on a weighting appropriate for the local terrain distortions applicable within each contributing image product. This opens the door to seamless composites using data from multiple imaging modes and satellites. We demonstrate here how composites can be generated automatically over large regions. More generally, they have seen application as an *analysis ready* product [31], [32] for a wider variety of users investigating land cover time series for applications such as forest classification [33], storm-driven windthrow in forests [34], or estimating melt onset [35].

A. Local Contributing Area

Recall how during RTC product generation, knowing the local area was necessary in order to properly calculate the normalized radar cross section in the gamma nought convention under consideration of terrain. That local area can also be terrain geocoded for every acquisition, so after GTC and RTC processing one can have the GTC backscatter, RTC terrain-flattened gamma nought backscatter, and the local area—all in map geometry.

An example of two sets of GTC/Area/RTC product groups is illustrated in Fig. 4. The swissALTI3D height model [36] was used for processing with 10 m postings. An ascending acquisition is shown in the top row, a descending acquisition in the bottom row. The dark regions are Lake *Thun* in the west and Lake *Brienz* in the east, with the city of *Interlaken* located directly between the lakes. Note how the foreslopes are clearly visible on one side of the hills in the GTC/Area images for the ascending case, and the opposite in the descending case. Similarly, the small black radar shadow regions are generally visible in one location in the ascending case, and a different one in the descending (see RTC and Area images). RTC images mark regions affected by radar shadow with a null-cell-value, as no backscatter estimate is possible there.

By combining RTC products generated from images acquired in different geometries, one is able to produce a composite backscatter image where such radar-shadow artifacts are strongly mitigated. Note that radar shadow is not common in Sentinel-1 geometries: the example shown contains some of the steepest terrain in Europe, particularly the *Lauterbrunnen* valley south of Interlaken.

B. Local Resolution Weighting

Users of radar data should be aware of the fact that the local area observed is inversely proportional to the local image resolution [37]. So, if one generates a composite with multiple coregistered inputs, whereby the inverse of the local area is used to weight the contribution of each input image, one has weighted each image by its local resolution. Given a local set of M nonshadowed input RTC image samples $\gamma_1^0 \ldots \gamma_M^0$, for each image i with a local area A_i, the sum of the available resolutions is

$$S_r = \sum_{j=1}^{M} \frac{1}{A_j}. \tag{3}$$

The weight W_i to be applied to each image i is then

$$W_i = \frac{1}{A_i} \cdot S_r. \tag{4}$$

Given that all weights $W_1 \ldots W_M$ are now available, for any given map geometry sample location, the composite's backscatter estimate γ_c is the weighted sum of all M available input RTC backscatter values [37], [38]

$$\gamma_c = \sum_{i=1}^{M} W_i \cdot \gamma_i^0. \tag{5}$$

Input images where the location in question is subject to radar shadow are *not included*, as they do not offer an observation. In those cases, the number of available images M is locally smaller and the weights account for that. A flowchart outlining the processing scheme is shown in Fig. 6. From the DHM and SAR backscatter inputs, image simulation is used to estimate the local illuminated area in radar geometry,

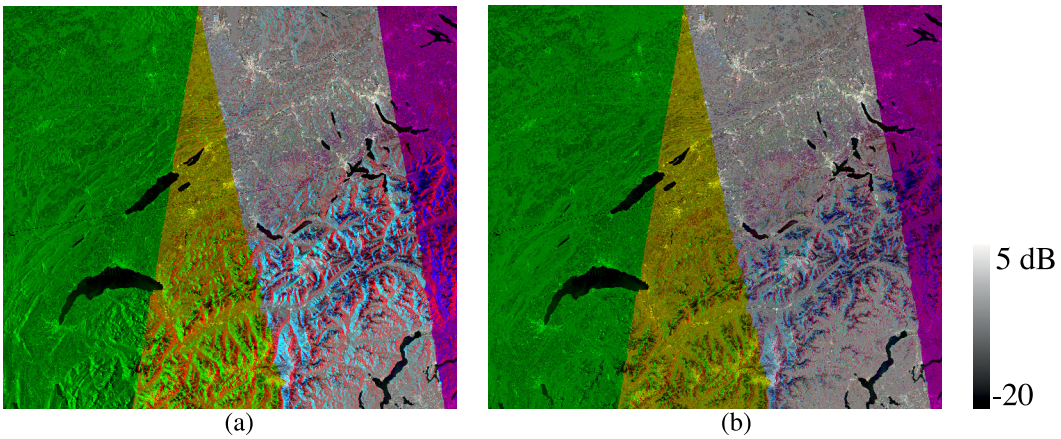

Fig. 3. Comparison of temporal signature in S-1. (a) GTC vs. (b) RTC VV-pol. backscatter overlays for IW acquisitions over Switzerland from 2017.04.27-29; Swiss map projection; Red = 2017.04.27 05:33; Green = 2017.04.28 17:21; Blue = 2017.04.29 17:14–contains modified Copernicus Sentinel data (2017).

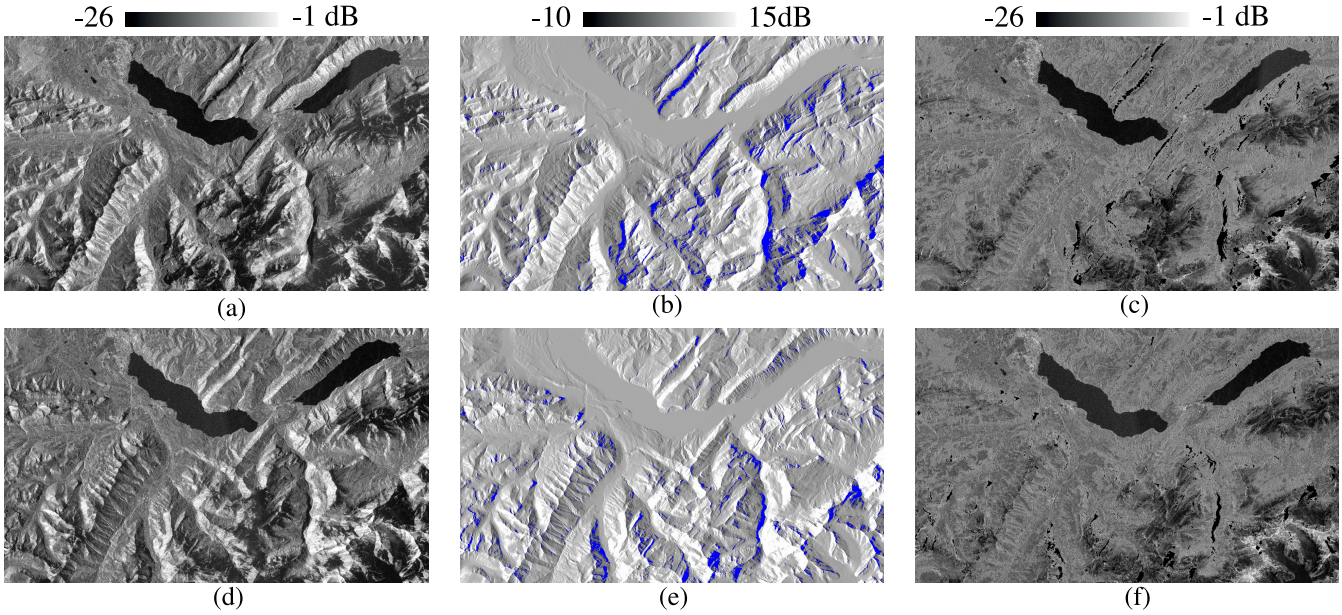

Fig. 4. GTC (left), Local Area with shadow marked blue (middle), RTC (right) for Sentinel-1 IW GRDH descending (top, 2015.05.26) and ascending (bottom, 2015.05.267) acquisitions–region surrounding Interlaken, Switzerland-Swiss oblique Mercator-VH-pol. swissALTI3D DEM applied–contains modified Copernicus Sentinel data (2015). (a) GTC γ^0_E 2015.05.26. (b) Local area 2015.05.26. (c) RTC γ^0_T 2015.05.26. (d) GTC γ^0_E 2015.05.27. (e) Local area 2015.05.27. (f) RTC γ^0_T 2015.05.27.

then used to normalize the backscatter. Both the normalized backscatter and the area are terrain-geocoded. A set of areas and backscatter maps corresponding to a set time window are then integrated into a single backscatter map for a region of interest.

By applying the above equations given the two sets of Sentinel-1 Area/RTC images shown in Fig. 4, one is able to generate the composite shown in Fig. 5. One can see that the radar shadow regions (black in the input RTC images) do not appear in the composite, as they only very rarely are colocated in multiple input images. This leads to both sides of the hills and mountains being well resolved, as the effects of foreshortening and layover are strongly mitigated.

In this simple example, the number of input images was $M = 2$. But the technique can be applied with a larger number of input images: all available images that satisfy membership within the specified (a) spatial extent and (b) time window, can contribute to the local composite backscatter value. By increasing the number of images, one is able to extend full coverage and further lower the noise in the output composite. Lowering the noise is particularly important when working at the full resolution of the sensor. The composites are L3 products, expressed on a uniform spacetime grid scale [3], [39].

The top row of Fig. 7 juxtaposes simple mosaics following the σ^0_E and γ^0_E conventions, respectively. As radiometric terrain effects are not compensated, edge effects are prominent at the cutover between different sources. In Fig. 7 at bottom-left, one sees that an RTC has much-improved behavior in the mountains. Though not visible at this scale, variations in local resolution remain. In Fig. 7 at the bottom right, the LRW backscatter is shown, whereby all available data

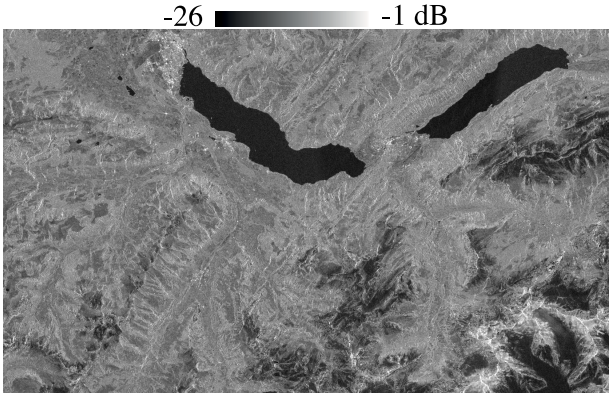

Fig. 5. LRW VH-pol. backscatter composite generated with ascending/descending combination of Sentinel-1 IW acquisitions of 2015.05.26 and 2015.05.27-Interlaken, Switzerland–Swiss map coordinates-swissALTI3D DEM applied–contains modified Copernicus Sentinel data (2015).

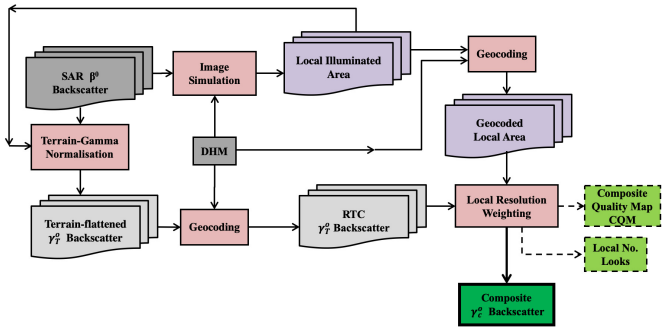

Fig. 6. Flowchart of LRW Backscatter Composite Processing starting with inputs DHM and SAR β^0 backscatter.

sets were integrated to produce the composite. In the overlap region, the local resolution became more consistent, with fewer poor-quality outliers.

C. Local Quality: Number of Observations

Depending on the time window length and the number of tracks where a SAR sensor observes a specific region within the coverage area, the number of observations can vary significantly across a single LRW-backscatter map. Radar shadow can also reduce the number of local observations in areas affected by steep terrain. A map of the number of observations that were used to generate a backscatter composite can be useful as a potential auxiliary product to document variations in the quality of the composite generated. Examples of such auxiliary products are illustrated in Fig. 8. Fig. 8(a) shows the local number of observations in the case of a 4-day window, while Fig. 8(b) shows the same for a 6-day window. Note how widening the observation window by two days significantly increased the number of independent observations available for integration within the composite. Widening the temporal window improves the number of observations available, but also increases susceptibility to the introduction of uncertainties caused by natural variability within the time span of the window. That can potentially make interpretation of the composite backscatter value more difficult, so narrow time windows are preferred when possible.

These maps are useful as a qualitative map of possible variations in the quality of the composite, but they do not differentiate between ascending and descending observations, nor do they give a direct indication of the locally valid resolution within the composite. We propose a further auxiliary product to help map those variations.

D. Local Quality: Composite Local Resolution

A more quantitative auxiliary product that would be potentially useful to document variations in quality within an LRW-backscatter mosaic is illustrated in Fig. 8(c) and (d). These are composite quality maps (CQM), calculated in a manner similar to the calculation of the backscatter composite itself. The map expressed in dB is calculated as

$$\mathrm{CQM} = -10 \cdot \log_{10}\left(\sum_{i=1}^{M} W_i \cdot A_i\right). \tag{6}$$

Rather than applying the weights to each input RTC image, for these products, the weights are instead applied to the local contributing areas (originally used to generate the RTC products) to produce a map of the weighted relative area within the LRW-composite. High values indicate relatively high (good) resolution, low values indicate relatively coarse local resolution.

Composite quality maps give a better indication of local quality, as they provide a finer account of the local availability (or not) of high-quality observations. Note in Fig. 8(c) how the local resolution remains poor in mountainous regions when only ascending or only descending observations are available. When both ascending and descending observations are available for combination, then the local variations in the resolution are reduced, and the composite's quality becomes more homogeneous. The types of variations seen in Fig. 8(c) would be cause for concern, and one might need to consult the auxiliary product to ensure that an analysis conducted on the composite would be valid in the region of interest. However, once relative homogeneity is achieved such as that seen in Fig. 8(d), then the auxiliary product can serve as a "green light" indicating that 2-D analysis across the wide region covered by the whole composite can be applied without significant reservation. Fig. 9 shows the distribution of CQM for elevations above 1000 m in the western alps given acquisitions over (a) 4 days, and (b) 6 days versus the local slope. Note that the 4-day case includes many points lower than -3 dB, while after 6-days most of those poor quality points were improved to above that level. As expected, steep slopes exhibit even higher quality than flatter regions, as the back-slope acquisitions dominate there locally, with high local resolution. In the steepest slopes, the low number of such observations made the calculation of the median erratic. A log scale was applied here; the actual improvement in *linear* backscatter is even more pronounced.

IV. Discussion

A. Input SAR Product Resolution

The LRW-approach can be used to integrate products from different sensors and modes into a single 2-D backscatter map.

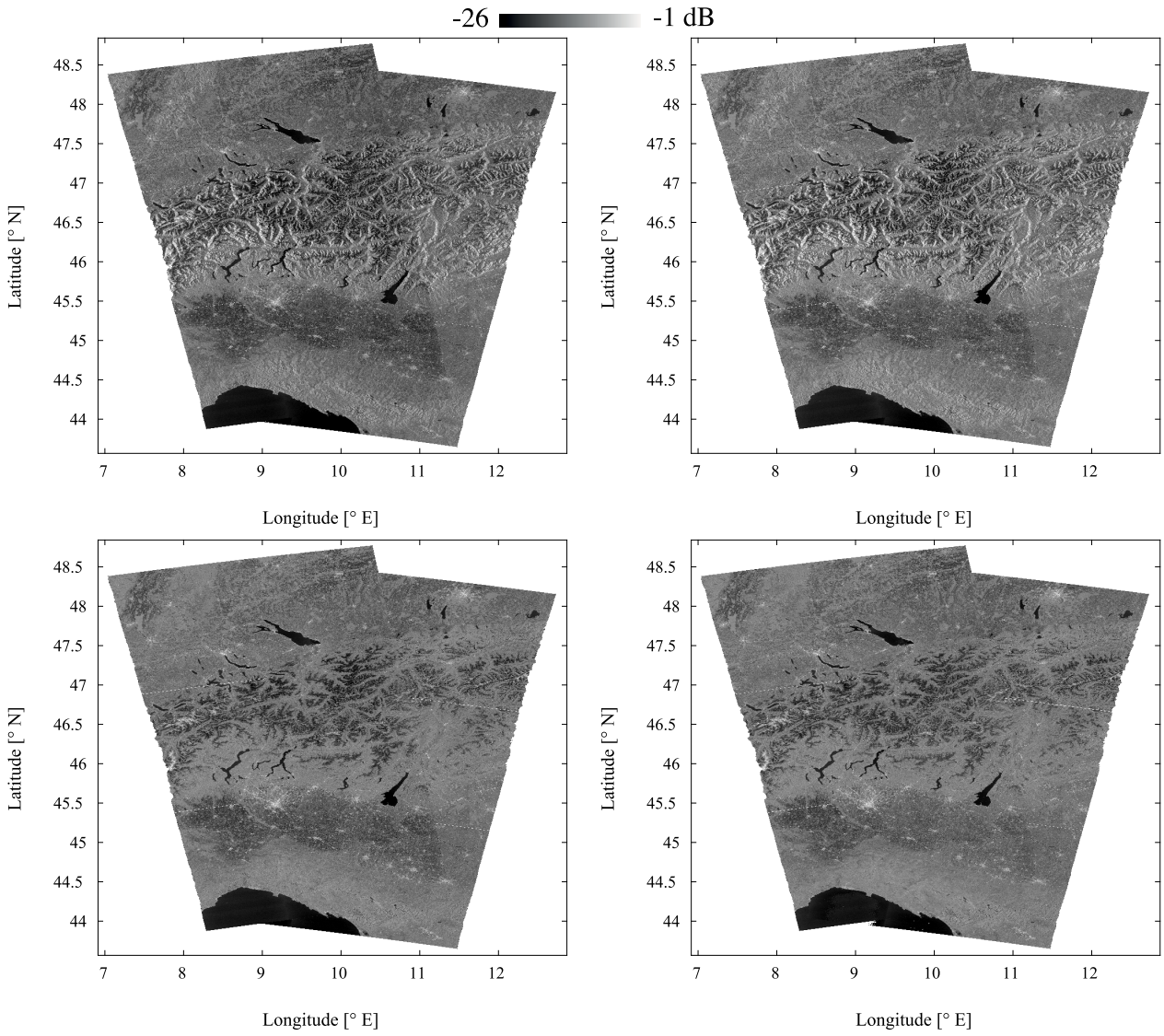

Fig. 7. Sigma nought versus Gamma nought in the Alps-Sentinel-1A ascending/descending 2016.05.03-04-SRTM DEM applied–(top-left) σ_E^0 mosaic, (top-right) γ_E^0 mosaic, (bottom-left) γ_T^0 mosaic, (bottom-right) γ_c^0 composite–contains modified Copernicus Sentinel data (2016).

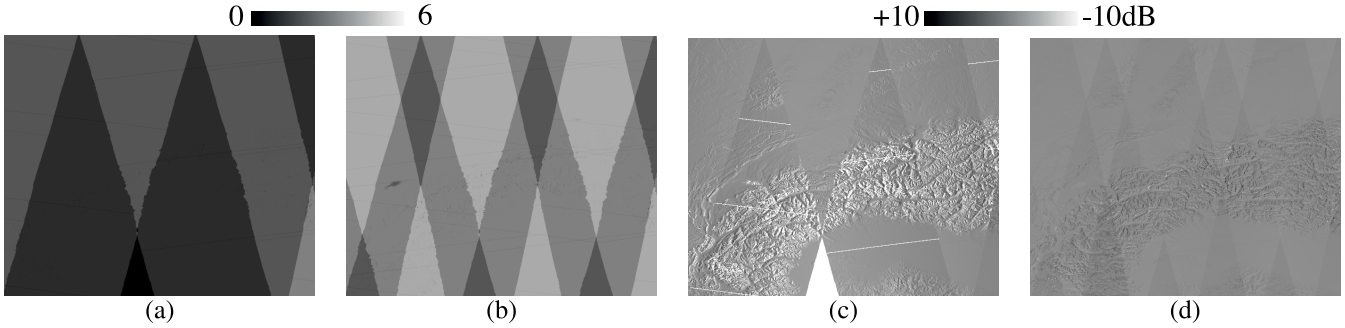

Fig. 8. Potential auxiliary products-Number of local observations versus CQM-Western Alps. (a) No. of local observations in 4-day LRW. (b) No. of local observations in 6-day LRW. (c) CQM 4-day LRW. (d) CQM 6-day LRW.

Different L1 processing schemes can also be accommodated: e.g., if users prefer detected L1 single-look-complex (SLC) products presented in slant range as input, they can be used instead, or even "mixed" with ground range detected (GRD) products. Cases can arise where a set of contributing modes have different inherent resolutions. For example, one might wish to mix S-1 IW GRDH (10 m samples) and Extra Wide-swath (EW) GRDM (40 m samples) into a single

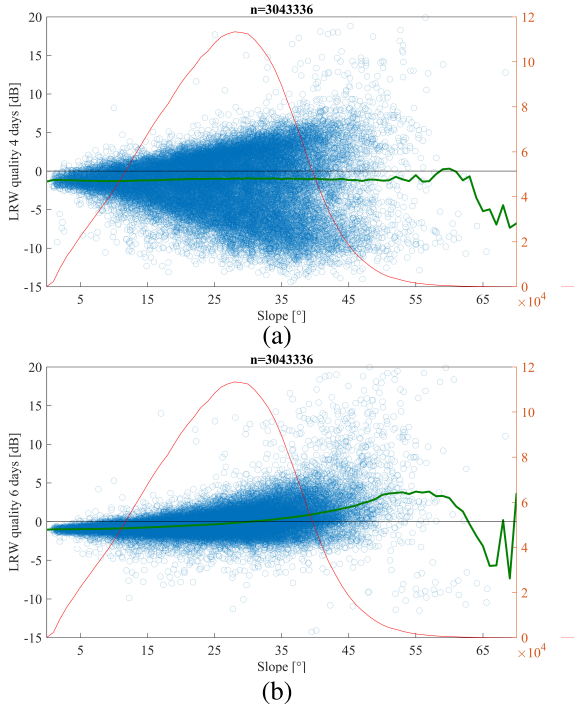

Fig. 9. Composite Quality versus slope for (a) 4-day and (b) 6-day composites over Western Alps at elevations above 1000 m–Green line is median, red shows number of occurrences with given slope in data set.

composite product. Then the user must decide how to treat the uneven input image resolutions. One can (a) undersample the IW-GRDH data to the same sample rate as GRDM and proceed with a uniform input sample interval, or (b) oversample the GRDM data into the higher sampling rate available in GRDH data. In the following, we chose the former option in order to reduce the data volume. Other use cases might favor other options.

B. Composite Backscatter Resolution

It is important to recall that the backscatter composite has a better mean spatial resolution than any one of the input SAR images used to generate it. This is the case because the LRW prefers to use information from the back-slopes (with high local resolution) in comparison to fore-slopes (with very poor local resolution due to foreshortening/layover). As a bonus, back-slopes provide more looks (more independent observations). The noise characteristics of the composite backscatter product are therefore superior to those of the individual input products due to (a) more looks per image and (b) integration of information from more images. The composites can be based on backscatter values with or without denoising applied [40], [41] at the L1 input stage. In a manner similar to the CQM, composite "noise maps" generated using the same weights applied to make the backscatter composite could provide guidance on local noise levels.

C. Multisensor Integration

The LRW compositing approach enables the integration of observations from multiple radar modes [e.g., Sentinel-1 IW and EW or Radarsat-2 ScanSAR Wide Swath Beam Combination A (SCWA)] but also from different sensors. In cases where the sensors observe at the same wavelength [e.g., Sentinel-1 (S-1) and Radarsat-2 (RS2) or Radarsat Constellation Mission (RCM)], then given that all sensors meet consistently high standards of geometric and radiometric calibration, the LRW-backscatter composites can benefit from an increased diversity of viewing geometries rather than suffer from it, as is the case in single-track analyses or InSAR combinations that require repeat passes. For example, S-1 data crossed with RS2 or RCM will not likely be able to offer systematic InSAR pairs, but their L1 backscatter products can be combined into hybrid backscatter maps using the LRW approach.

An example of the differences between evaluations of a region given data only from a single sensor, or by integrated calibrated "hybrid" multisensor retrievals is shown in Fig. 10. A DEM based on the Canadian DEM (CDED) data set [42] was used during RTC product generation. For the period of August 2–3, 2016, in Fig. 10(a), an LRW-backscatter composite of Ellesmere island is shown that was based on RS2 data only. In Fig. 10(b), an LRW-backscatter composite is shown for the same region and time period that was based on S-1A data alone. S-1B had not yet been commissioned when these data were acquired. S-1A mainly covered only the southern part of the region, and RS2 mainly the eastern central portion.

In Fig. 10(c) an integrated LRW taking data from both S-1A and RS2 is shown. This is the first known instance of a composite based on calibrated *multisensor SAR* input. Each sensor's tracks have individual terrain-induced distortions that were first corrected (RTC product generation) and then used to locally weight each sensor's contribution to the composite (LRW ARD product generation). The coverage is much wider than either in isolation. Note that no obvious "edge" effects are visible at the boundary between S-1A and RS2 acquisitions. LRW products from our processor were recently used to demonstrate that single-day temporal resolution is becoming possible with SAR sensors [35], becoming competitive with the coverage and revisit of passive microwave and scatterometer sensors while providing orders of magnitude of improvement in spatial resolution. Multiple sensors can be combined at appropriate "Application Readiness Levels" (ARL), as introduced in [43]. ARL-1 through ARL-3 categorize sensors according to their compatibility. Seamless ARL-3 backscatter coverages of the types shown here are well suited to the direct integration of multiple virtual constellations for regional or global terrestrial monitoring.

D. Seamless Wide-Area Composites

Users of a radar composite need not always know the ultimate origin of each backscatter observation used to build up the 2-D maps they analyze. These composites are not simple "mosaics" of independent images, but actual merged composite outputs, wherein overlapping regions the quality of the composite improves upon the individual inputs. Note that no "feathering" was applied at the edges between individual acquisitions: a hard cutover was always applied. The guarantor for the lack of edge effects between individual acquisitions is

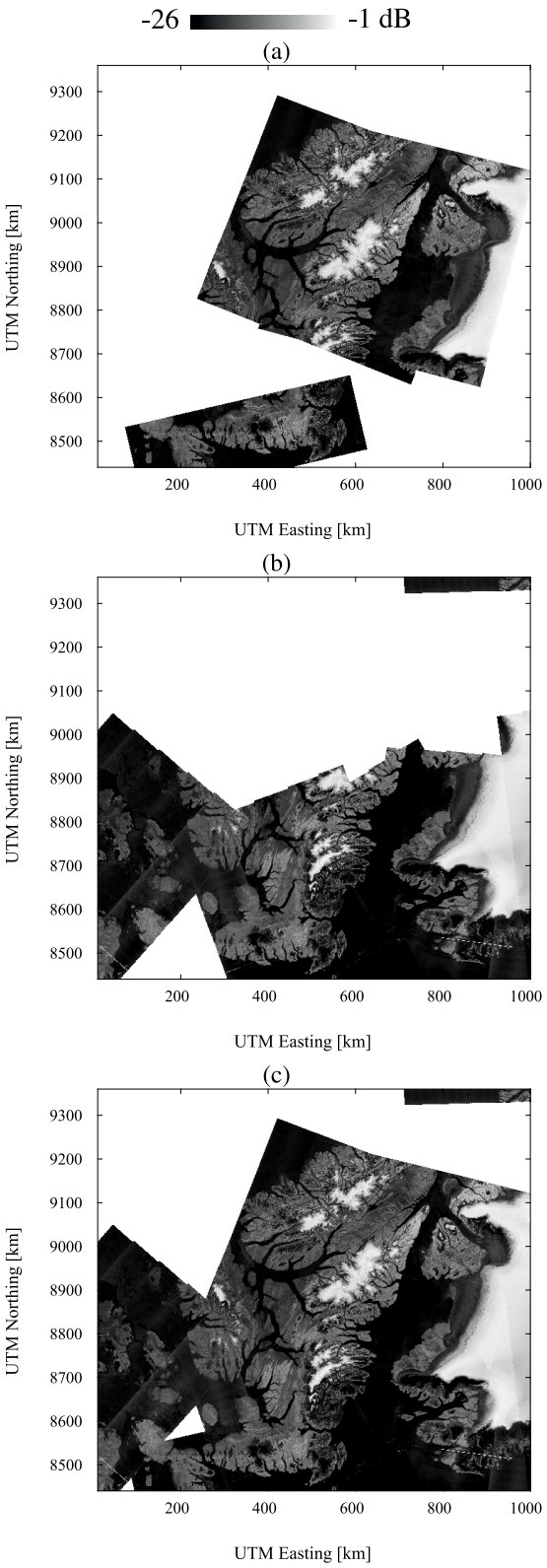

Fig. 10. Single versus multisensor HV-pol. backscatter composites-(unobserved voids white)-August 2–3, 2016-Ellesmere Island, Nunavut, Canada-(a) RS2 only (SCWA), (b) S-1A only (EW), (c) S-1A combined with RS2-Universal Transverse Mercator (UTM) zone 22 map projection–contains modified Copernicus Sentinel data (2016)-RADARSAT-2 Data and Products MacDonald Dettwiler and Associates Ltd. (2016)-All Rights Reserved. RADARSAT is an official trademark of the CSA.

that both data sources meet strict geometric and radiometric calibration requirements [24], [44]. The method is applicable to single, dual- or quad-pol data sets, and not dependent on the availability of the full scattering matrix [45].

Proper terrain-corrections ensure that no significant beam-edge artifacts are visible. Being able to combine data from multiple radar sensors could offer 1–2 day temporal resolution over wide regions, opening up research questions and applications that base their analysis on 2-D change detection to wide-area coverage. It is also more cost-effective to cooperate among space agencies, as services built on their satellite constellation become less sensitive to a single point of failure.

Examples of wide-area composites covering the whole of the European Alps are shown in Fig. 11. Alpine wide-area mosaics have been generated since the first release of Sentinel-1A data in Oct. 2014. In the following, we show three sample images illustrating the seasonal progression of snow melting in the Alps from Jan. through May 2017. In these cases, first 10×10 multilooking was applied to the input GRDH products, RTC processing was performed, and LRW was applied. This was performed for a set of (overlapping) time windows. In the first example, a time-window of 12 days was used. Fig. 11 shows a series of three wide-area backscatter composites calculated using the LRW approach. The backscatter range was set identically for all 3 RGB channels (-21 to -6 dB). A 12-day window length was applied. Note how relatively high backscatter is seen during the winter in Fig. 11(a), with melting (lower backscatter) evident in the March image seen in Fig. 11(b). The melting is seen to be more intense and extends also to higher elevations by May, as seen in Fig. 11(c). The progression of melting from lower elevations to higher is made even clearer in the RGB-overlay of three 12-day composites shown in Fig. 12. The highest peaks appear yellow, as their backscatter remained high (from the dry snow present locally) in the first two time-windows (bright red and green channels), only reducing in the final composite (dark blue channel). Short time windows can increase the probability of parts of the composite having a "single source", which can increase the likelihood of having a visible edge within a composite.

E. Wet Snow and Ice Mapping

Optical sensors see snow clearly in the absence of clouds, but they are not able to differentiate well between dry and wet snow. C-band radar sensors provide an extra layer of information: the backscatter they receive is modulated strongly by wet snow [46], while dry snow is often nearly transparent.

Mapping wet snow is important for hydrology [47] and run-off models [48]. Mapping wet snow particularly in the *mountains* is important, as (a) that is where snow lies for extended periods, and (b) snow-laden mountains provide a water source to many people for many months when alternative sources are not easily accessible [49]. LRW backscatter composites provide wide area coverage with an otherwise unknown combination of high geometric accuracy, radiometric calibration, and consistent local resolution. Wet snow has traditionally been mapped by comparing new incoming "candidate" images with a dry cold reference backscatter image, and delineating image regions where the backscatter

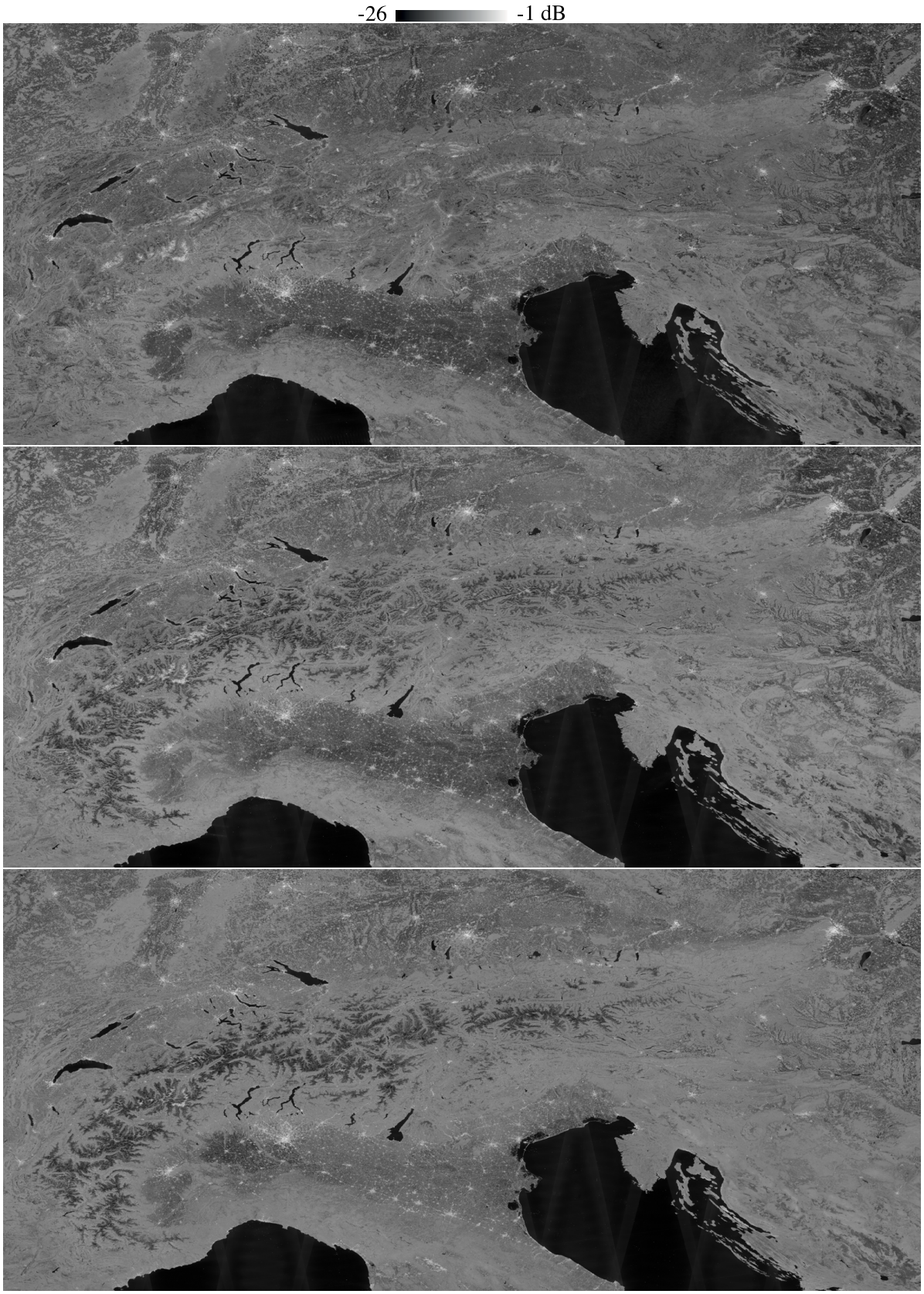

Fig. 11. Time series of wide-area Sentinel-1 VH-pol. backscatter composites with 12 day time windows in 2017 covering the Alps–(a) 2017.01.01-12, (b) 2017.03.26-04.06, (c) 2017.05.13-24–Lat/Lon 43.5-49° N; 5.5-17.5° E–SRTM applied—contains modified Copernicus Sentinel data (2017).

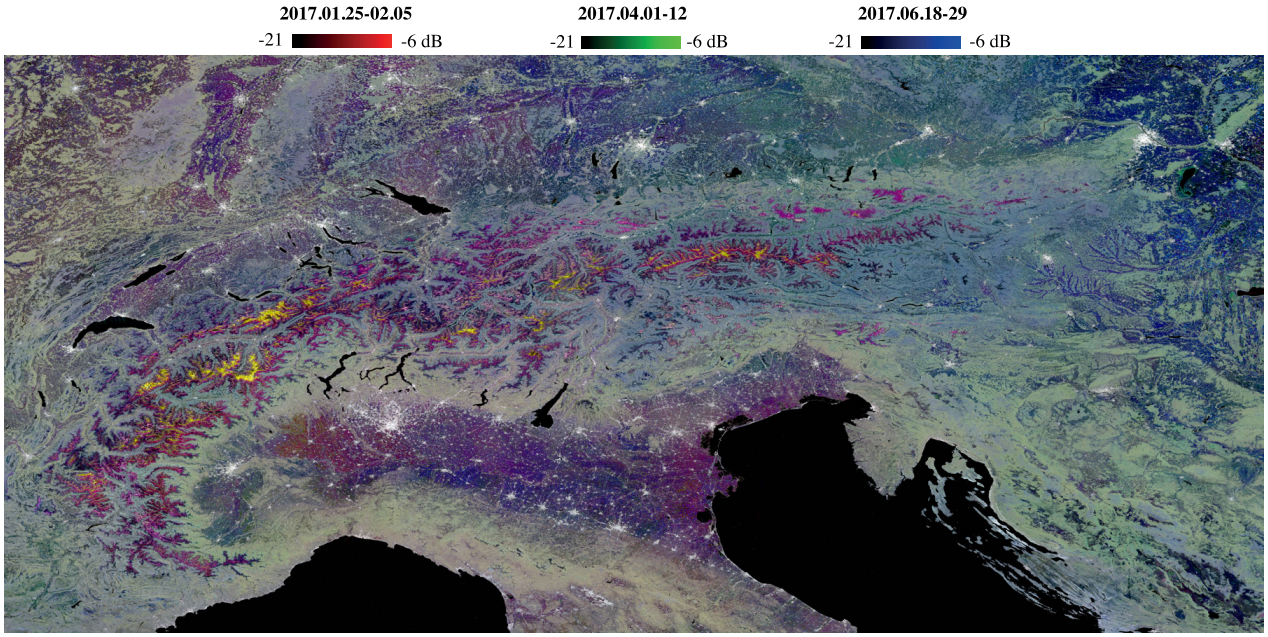

Fig. 12. Alpine snow melt visualized in RGB overlay of three LRW Sentinel-1 VH-pol. backscatter composites; each color channel corresponds to the following date ranges—Red: 2017.01.25-02.05, Green: 2017.04.01-12, Blue: 2017.06.18-29—Lat/Lon 43.5-49° N; 5.5-17.5° E—SRTM applied—contains modified Copernicus Sentinel data (2017).

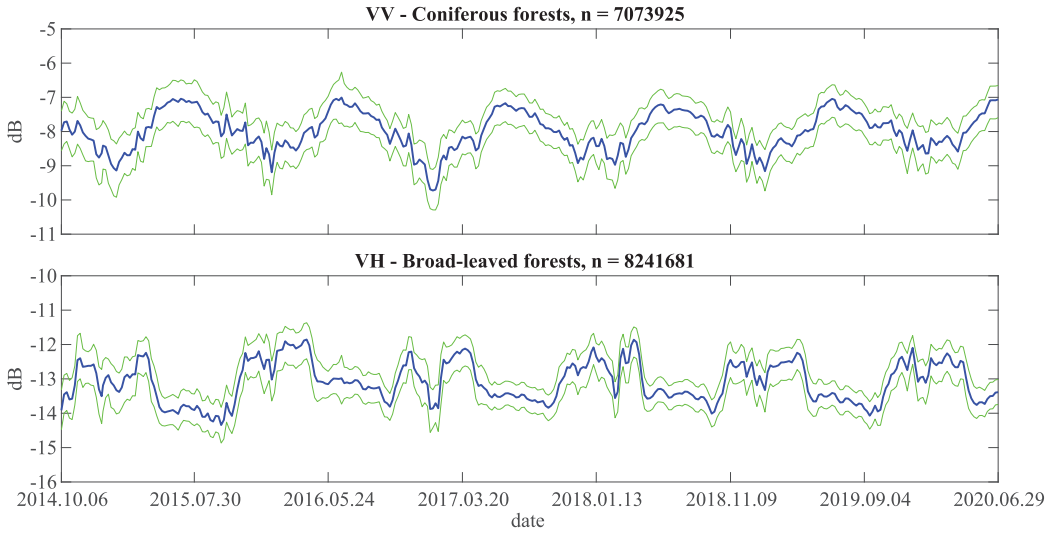

Fig. 13. Alpine forest time series. (Top) Sentinel-1 VV-pol. backscatter from coniferous forests. (Bottom) VH-pol. backscatter from broad-leaved forests. The number of investigated pixels (n) was comparable for both forest types—medians in blue, quartiles in green-Lat/Lon 43.5-49° N; 5.5-17.5° E—contains modified Copernicus Sentinel data (2014–2020).

is significantly lower than the reference [50], [51]. This relies on a stream of strictly single-track acquisitions, with dry cold reference images precalculated for each track [52], [53]. The temporal resolution is tied to the repeat-pass interval. Studies of requirements for snow products in the past [7], [54] have requested *daily* temporal resolution–however, this has never been achieved over wide areas: neither with optical sensors (due to cloud cover) nor radar (due to longer revisit intervals). Using LRW wide-area composites, one is able to provide maps with large spatial coverage with the temporal resolution not directly tied to the orbital repeat interval, while simultaneously ensuring use of a consistent dry cold reference and more homogeneous local resolution, especially in mountainous regions [55], [56].

F. Land Cover Monitoring

Fig. 13 illustrates a longitudinal time series of backscatter signatures retrieved from LRW composites covering the Alps from 2014 to 2020. Backscatter from CORINE land cover 2018 [57] forest class regions were extracted after 3×3 erosion to reduce edge contamination. The backscatter statistics for each forest type were then evaluated through time. As seen in Fig. 13(top) the conifer VV-pol. backscatter regularly rises in the summer and falls in the winter, possibly due to needle

growth [33]. A seasonal trend with an opposite phase is seen in VH-pol. within broad-leaved forests in Fig. 13(bottom). This may be caused by stronger backscatter from branches and/or a stronger ground scattering component in the leaf-off state [33]. Thaw events occasionally introduce ambiguity in midwinter, esp. in VH-pol. Quartile backscatter intervals are marked in green above and below the blue median. Similar backscatter trends were reported in local Alpine test sites in [33] and [58]. Backscatter composites generated via this LRW method have been successfully used to monitor the phenology and classify different types of forest [33] and for change detection on short time scales, e.g., to detect windthrow in forests after a storm [34]. Achieving a seasonal overview of Alpine conifer backscatter would be more challenging using single-track approaches based on L1 products [3], but it becomes a relatively quick task given the availability of L3 [3] backscatter composites. Single-track approaches do not integrate information from other viewpoints and are hence subject to higher noise levels.

V. Conclusion and Recommendations

We demonstrated backscatter composites that fulfill the definition of L3 products [3]. LRW composites are generated on *uniform space-time scales*, have *completeness and consistency properties* (seamless wide-area coverage with RTC), and cover *complete regions mosaicked together from multiple orbits*. To our knowledge, no previously proposed backscatter mosaicking methodology has fulfilled these criteria, often lacking RTC and always exhibiting inconsistent geometric resolution over areas with steep terrain. Our methodology is also the first to demonstrate seamless multisensor integration.

Space agencies have until now developed constellations that included a maximum of a few radar imaging platforms. With "new space", we are entering an era with possibly larger constellations [59]–[61] (e.g., ICEYE [62], [63], Capella Space [64]) and this may enable the attainment of daily coverage (at X-band) by combining data acquired in different geometries. Only limited spatial coverage will be possible in cases where solely spotlight or stripmap *narrow*-swath acquisitions are available-it will be possible to extend the size of the region covered at a high temporal resolution if instead predominantly *wide*-swath acquisitions are available [e.g., ScanSAR or Terrain-Observation with Progressive Scans SAR (TOPSAR)]. Using wide-swath modes, operators are encouraged to exploit a nominal incident angle range that endeavors to stay within a consistent backscatter regime (e.g., as Sentinel-1 IW). In the future, there will likely be a trend to naturally introduce this data into the mix of existing institutional data streams. These trends underline again the need for powerful techniques for constructing composites.

Comparing the two major methods of wet snow detection, one may note the following. Ensuring that ascending/descending acquisitions are acquired close in time allows composites generated from their data to maintain a narrow time-tag [65]. Single-track/mode methodologies are tied to a single sensor setting and best suited to "data poor" environments. Backscatter composite methodologies are open to combining inputs from multiple SAR sensors and modes, whether that be e.g., IW + EW in the S-1 case, or S-1 IW + EW + RS2 SCNB + SCWA (ScanSAR Narrow Beam Combination B and ScanSAR Wide Beam Combination A). They are best suited to "data rich" environments. Multiple beam modes may even be acquired in different tracks/relative orbits. Diversity in the details of the acquisition modes being integrated is not a hindrance. On the contrary, it can provide extra information, e.g., by providing measurements in mountain valleys in perpetual radar shadow given only a different sensor's set of available geometries. Although backscatter composites from LRW show their largest benefits in mountainous regions where the high resolution on backslopes is harnessed, they do not lose applicability also in comparative flatlands. In flat smooth terrain, differences caused by individual viewing geometries may remain apparent (e.g., copol. Bragg scattering on water). Depending on their relative strength, without further corrections, these may hinder interpretation of local backscatter behavior in the composite, detracting from the "analysis readiness" of the L3 data set.

The following recommendations are made:

1) Over mountainous regions, radar satellite acquisition plans should stress ascending/descending tracks to be planned with as little delay as possible to ensure temporal coherency (these requirements can vary with application-e.g., for wet snow: daily).
2) Consideration should be given to adding level 3 [3] analysis ready wide-area backscatter composites to the standard product families of radar satellites.
3) Space agencies may consider consulting with each other to define a possible test region with a harmonized acquisition pattern [65] for the study of improvements to composite backscatter temporal resolution. For example, were the full complement of S-1 and RCM satellites to participate in monitoring a springtime melt process over a mountainous region, the temporal resolution would be significantly improved. Improving the temporal resolution will be advantageous in capturing leaf emergence, monitoring leaf fall, and generally in change detection (e.g., mapping wet snow or windthrow).

By adding wide-area calibrated geocoded backscatter products to their standard offerings, space agencies would make their data much more accessible to a wide spectrum of users, encouraging the development of new applications.

Acknowledgment

The authors wish to thank the European Space Agency (ESA) and the Copernicus Program for the Sentinel-1 data, as well as the Canadian Space Agency (CSA) and MacDonald Dettwiler and Associates (MDA) for the use of the Radarsat-2 data. The authors would also like to thank in particular are due to Stephen Howell and Mike Brady of Environment and Climate Change Canada and Yves Crevier of CSA for arranging access to the Radarsat-2 data. RADARSAT-2 Data and Products MacDonald Dettwiler and Associates Ltd. (2016)-All Rights Reserved. RADARSAT is an official trademark of the CSA. Figures contain modified Copernicus Sentinel data (2014–2020). The authors would also like to thank the reviewers for their highly constructive comments.

REFERENCES

[1] C. O. Justice *et al.*, "An overview of MODIS land data processing and product status," *Remote Sens. Environ.*, vol. 83, nos. 1–2, pp. 3–15, Nov. 2002.

[2] NASA. (2020). *MODIS Data Products*. Accessed: Sep. 25, 2020. [Online]. Available: https://modis.gsfc.nasa.gov/data/dataprod/

[3] NASA, "Report of the EOS data panel," NASA, Washington, DC, USA, Tech. Rep. Technical Memorandum 87777, 1986, vol. IIa, ch. II, p. 5.

[4] A. Schubert, M. Jehle, D. Small, and E. Meier, "Mitigation of atmospheric perturbations and solid Earth movements in a TerraSAR-X time-series," *J. Geodesy*, vol. 86, no. 4, pp. 257–270, Apr. 2012.

[5] A. Schubert, N. Miranda, D. Geudtner, and D. Small, "Sentinel-1A/B combined product geolocation accuracy," *Remote Sens.*, vol. 9, no. 6, p. 607, Jun. 2017.

[6] C. Gisinger *et al.*, "In-depth verification of Sentinel-1 and TerraSAR-X geolocation accuracy using the Australian corner reflector array," *IEEE Trans. Geosci. Remote Sens.*, vol. 59, no. 2, pp. 1154–1181, Feb. 2021.

[7] K. Alverson and B. Ryan, "Cryosphere theme report," Meteorol. Org., Integr. Global Observing Strategy, Tech. Rep., 2007.

[8] D. Small, "Flattening gamma: Radiometric terrain correction for SAR imagery," *IEEE Trans. Geosci. Remote Sens.*, vol. 49, no. 8, pp. 3081–3093, Aug. 2011.

[9] E. Meier, U. Frei, and D. Nüesch, "Precise terrain corrected geocoded images," in *SAR Geocoding: Data and Systems*. Berlin, Germany: Wichmann Verlag, 1993, pp. 173–186.

[10] D. Small, A. Schubert, B. Rosich, E. Meier, B. Rosich-Tell, and E. Meier, "Geometric and Radiometric Correction of ESA SAR Products," in *Proc. ESA Envisat Symp.* Montreux, Switzerland: ESA, Apr. 2007, pp. 1–6.

[11] A. Schubert, D. Small, N. Miranda, D. Geudtner, and E. Meier, "Sentinel-1A product geolocation accuracy: Commissioning phase results," *Remote Sens.*, vol. 7, no. 7, pp. 9431–9449, Jul. 2015.

[12] A. Schubert, M. Jehle, D. Small, and E. Meier, "Geometric validation of TerraSAR-X high-resolution products," in *Proc. TerraSAR-X Sci. Team Meeting*. Oberpfaffenhofen, Germany: DLR, 2008, p. 6.

[13] G. M. Foody, "An assessment of the topographic effects on SAR image tone," *Can. J. Remote Sens.*, vol. 12, no. 2, pp. 124–131, Dec. 1986.

[14] T. Bayer, R. Winter, and G. Schreier, "Terrain influences in SAR backscatter and attempts to their correction," *IEEE Trans. Geosci. Remote Sens.*, vol. 29, no. 3, pp. 451–462, May 1991.

[15] J. M. Kellndorfer, L. E. Pierce, M. C. Dobson, and F. T. Ulaby, "Toward consistent regional-to-global-scale vegetation characterization using orbital SAR systems," *IEEE Trans. Geosci. Remote Sens.*, vol. 36, no. 5, pp. 1396–1411, Sep. 1998.

[16] I. E. Mladenova, T. J. Jackson, R. Bindlish, and S. Hensley, "Incidence angle normalization of radar backscatter data," *IEEE Trans. Geosci. Remote Sens.*, vol. 51, no. 3, pp. 1791–1804, Mar. 2013.

[17] A. Loew and W. Mauser, "Generation of geometrically and radiometrically terrain corrected SAR image products," *Remote Sens. Environ.*, vol. 106, no. 3, pp. 337–349, Feb. 2007.

[18] O. Frey, M. Santoro, C. L. Werner, and U. Wegmuller, "DEM-based SAR pixel-area estimation for enhanced geocoding refinement and radiometric normalization," *IEEE Geosci. Remote Sens. Lett.*, vol. 10, no. 1, pp. 48–52, Jan. 2013.

[19] M. Simard, B. V. Riel, M. Denbina, and S. Hensley, "Radiometric correction of airborne radar images over forested terrain with topography," *IEEE Trans. Geosci. Remote Sens.*, vol. 54, no. 8, pp. 4488–4500, Aug. 2016.

[20] D. Small, S. Biegger, and D. Nüesch, "The topology of SAR imagery in rough topography," in *Proc. EUSAR*, Munich, Germany, May 2000, pp. 501–504.

[21] CEOS, "Analysis ready data for land (CARD4L)—Product family specification, normalised radar backscatter," CEOS CARD4L, Tech. Rep., 2020. [Online]. Available: http://www.ceos.org/ard

[22] ESA. (2020). *SNAP*. Accessed: Sep. 1, 2020. [Online]. Available: http://step.esa.int

[23] J. Truckenbrodt *et al.*, "Towards Sentinel-1 SAR Analysis-Ready Data: A best practices assessment on preparing backscatter data for the cube," *Data*, vol. 4, no. 3, p. 93, Jul. 2019.

[24] D. Small, L. Zuberbühler, A. Schubert, and E. Meier, "Terrain-flattened gamma nought Radarsat-2 backscatter," *Can. J. Remote Sens.*, vol. 37, no. 5, pp. 493–499, Oct. 2011.

[25] F. Wang, "Fuzzy classification of remote sensing images," *IEEE Trans. Geosci. Remote Sens.*, vol. 28, no. 2, pp. 194–201, Mar. 1990.

[26] D. H. Hoekman, M. A. M. Vissers, and N. Wielaard, "PALSAR wide-area mapping of borneo: Methodology and map validation," *IEEE J. Sel. Topics Appl. Earth Observ. Remote Sens.*, vol. 3, no. 4, pp. 605–617, Dec. 2010.

[27] G. D. De Grandi, A. Bouvet, R. M. Lucas, M. Shimada, S. Monaco, and A. Rosenqvist, "The K&C PALSAR mosaic of the African continent: Processing issues and first thematic results," *IEEE Trans. Geosci. Remote Sens.*, vol. 49, no. 10, pp. 3593–3610, Oct. 2011.

[28] M. Shimada *et al.*, "Generation of 10m resolution PALSAR and JERS-SAR mosaic and forest/non-forest maps for forest carbon tracking," in *Proc. IEEE Int. Geosci. Remote Sens. Symp.*, Jul. 2011, pp. 1–4.

[29] P. Soille *et al.*, "A versatile data-intensive computing platform for information retrieval from big geospatial data," *Future Gener. Comput. Syst.*, vol. 81, pp. 30–40, Apr. 2018.

[30] V. Syrris, C. Corbane, M. Pesaresi, and P. Soille, "Mosaicking copernicus Sentinel-1 data at global scale," *IEEE Trans. Big Data*, vol. 6, no. 3, pp. 547–557, Sep. 2019.

[31] CEOS, "CEOS future data access and analysis architectures study," CEOS, Tech. Rep., 2016. [Online]. Available: https://ceos-dev.ceos.org/document_management/Meetings/Plenary/30/Documents/5.2_Future-Data-Architectures-Interim-Report_v.1.pdf

[32] CEOS, "The CEOS data cube: Three-year work plan 2016–2018," CEOS, Tech. Rep., 2016. [Online]. Available: https://ceos-dev.ceos.org/document_management/Ad_Hoc_Teams/SDCG_for_GFOI/Meetings/SDCG-10/Cube%203-Year%20Work%20Plan%20-%20v1.0.pdf

[33] M. Rüetschi, M. Schaepman, and D. Small, "Using multitemporal Sentinel-1 C-band backscatter to monitor phenology and classify deciduous and coniferous forests in Northern Switzerland," *Remote Sens.*, vol. 10, no. 55, p. 30, Jan. 2018.

[34] M. Rüetschi, D. Small, and L. T. Waser, "Rapid detection of windthrows using Sentinel-1 C-band SAR data," *Remote Sens.*, vol. 11, no. 2, p. 23, Jan. 2019.

[35] S. E. L. Howell, D. Small, C. Rohner, M. S. Mahmud, J. J. Yackel, and M. Brady, "Estimating melt onset over arctic sea ice from time series multi-sensor Sentinel-1 and RADARSAT-2 backscatter," *Remote Sens. Environ.*, vol. 229, pp. 48–59, Aug. 2019.

[36] (2019). *Federal Office of Topography Swisstopo swissALTI3D*. Accessed: Sep. 4, 2019. [Online]. Available: https://shop.swisstopo.admin.ch/en/products/height_models/alti3D

[37] D. Small, "SAR backscatter multitemporal compositing via local resolution weighting," in *Proc. IEEE Int. Geosci. Remote Sens. Symp.*, Munich, Germany: IEEE Press, Jul. 2012, pp. 4521–4524.

[38] D. Small, M. Jehle, E. Meier, and D. Nüesch, "Radiometric terrain correction incorporating local antenna gain," in *Proc. EUSAR*, Ulm, Germany, May 2004, pp. 929–932.

[39] Wikipedia. (2020). *Remote Sensing Data Product Levels*. Accessed: Sep. 30, 2020. [Online]. Available: https://en.wikipedia.org/wiki/Remote_sensing/

[40] J.-W. Park, A. A. Korosov, M. Babiker, S. Sandven, and J.-S. Won, "Efficient thermal noise removal for Sentinel-1 TOPSAR cross-polarization channel," *IEEE Trans. Geosci. Remote Sens.*, vol. 56, no. 3, pp. 1555–1565, Mar. 2018.

[41] (2017). *Thermal Denoising of Products Generated by the Sentinel-1 IPF*. Accessed: Sep. 24, 2020. [Online]. Available: http://sentinel.esa.int

[42] M. Santoro and T. Strozzi, "Circumpolar digital elevation models >55° N with links to geotiff images," Gamma Remote Sensing, Pangaea, Tech. Rep., 2012, doi: 10.1594/PANGAEA.780111.

[43] M. A. Wulder *et al.*, "Virtual constellations for global terrestrial monitoring," *Remote Sens. Environ.*, vol. 170, pp. 62–76, Dec. 2015.

[44] A. Schubert, D. Small, M. Jehle, and E. Meier, "COSMO-skymed, TerraSAR-X, and RADARSAT-2 geolocation accuracy after compensation for earth-system effects," in *Proc. Int. Geosci. Remote Sens. Symp. (IGARSS)*. Munich, Germany: IEEE Press, Jul. 2012, pp. 3301–3304.

[45] O. Antropov, Y. Rauste, A. Lonnqvist, and T. Hame, "PolSAR mosaic normalization for improved land-cover mapping," *IEEE Geosci. Remote Sens. Lett.*, vol. 9, no. 6, pp. 1074–1078, Nov. 2012.

[46] W. I. Linlor, "Permittivity and attenuation of wet snow between 4 and 12 GHz," *J. Appl. Phys.*, vol. 51, no. 5, pp. 2811–2816, May 1980.

[47] M. Bavay, M. Lehning, T. Jonas, and H. Löwe, "Simulations of future snow cover and discharge in alpine headwater catchments," *Hydrol. Processes*, vol. 23, no. 1, pp. 95–108, Jan. 2009.

[48] Z. H. He, J. Parajka, F. Q. Tian, and G. Blöschl, "Estimating degree-day factors from MODIS for snowmelt runoff modeling," *Hydrol. Earth Syst. Sci.*, vol. 18, no. 12, pp. 4773–4789, Dec. 2014.

[49] D. Viviroli and R. Weingartner, "The hydrological significance of mountains: From regional to global scale," *Hydrol. Earth Syst. Sci.*, vol. 8, no. 6, pp. 1017–1030, Dec. 2004.

[50] T. Nagler and H. Rott, "Retrieval of wet snow by means of multitemporal SAR data," *IEEE Trans. Geosci. Remote Sens.*, vol. 38, no. 2, pp. 754–765, Mar. 2000.

[51] T. Nagler, H. Rott, E. Ripper, G. Bippus, and M. Hetzenecker, "Advancements for snowmelt monitoring by means of Sentinel-1 SAR," *Remote Sens.*, vol. 8, no. 4, p. 348, Apr. 2016.

[52] N. Baghdadi, "Capability of multitemporal ERS-1 SAR data for wet-snow mapping," *Remote Sens. Environ.*, vol. 60, no. 2, pp. 174–186, May 1997.

[53] H. Haefner and J. Piesbergen, "High alpine snow cover monitoring using ERS-1 SAR and Landsat TM data," in *Proc. IAHS Remote Sens. Hydrol.*, vol. 242, 1997, pp. 113–118.

[54] Z. Malenovský *et al.*, "Sentinels for science: Potential of sentinel-1, −2, and −3 missions for scientific observations of ocean, cryosphere, and land," *Remote Sens. Environ.*, vol. 120, pp. 91–101, May 2012.

[55] C. Rohner, "Relating snow wetness information gained from the intercantonal measurement and information system stations in Switzerland to Envisat ASAR backscatter," M.S. thesis, Dept. Geogr., Univ. Zurich, Zürich, Switzerland, 2014.

[56] D. Jäger, "Wide-area wet snow mapping of the Alps based on Sentinel-1 multi-track radar backscatter composites," M.S. thesis, Dept. Geogr., Univ. Zurich, Zürich, Switzerland, 2016.

[57] Copernicus. (2019). *Copernicus Data Product CLC2018*. Accessed: Aug. 30, 2019. [Online]. Available: https://land.copernicus.eu/pan-european/corine-land-cover/clc-2018/

[58] A. Dostálová, W. Wagner, M. Milenković, and M. Hollaus, "Annual seasonality in Sentinel-1 signal for forest mapping and forest type classification," *Int. J. Remote Sens.*, vol. 39, no. 21, pp. 7738–7760, Jun. 2018.

[59] P. Plourde *et al.*, "EO summit 2017: Challenges for next generation SAR," *Can. J. Remote Sens.*, vol. 44, no. 3, pp. 243–246, May 2018.

[60] G. Filippazzo and S. Dinand, "The potential impact of small satellite radar constellations on traditional space systems," in *Proc. Federated Fractionated Satell. Syst. Workshop*, vol. 5. Toulouse, France: ISAE SUP AERO, 2017, pp. 1–12.

[61] G. Seguin and D. Geudtner, "Challenges for next generation SAR," in *Proc. EUSAR*. Aachen, Germany: VDE, 2018, pp. 1350–1353.

[62] O. Antropov, J. Praks, M. Kauppinen, P. Laurila, V. Ignatenko, and R. Modrzewski, "Assessment of operational microsatellite based SAR for Earth observation applications," in *Proc. 2nd URSI Atlantic Radio Sci. Meeting (AT-RASC)*, May 2018, p. 1.

[63] P. Laurila, R. Modrzewski, T. Cheng, B. Campbell, and V. G. Yanni, "Validation of ICEYE small satellite SAR design for ice detection and imaging," in *Proc. Arctic Technol. Conf.*, 2016, pp. 1–10.

[64] G. Farquharson, W. Woods, C. Stringham, N. Sankarambadi, and L. Riggi, "The Capella synthetic aperture radar constellation," in *Proc. IGARSS - IEEE Int. Geosci. Remote Sens. Symp.*, Jul. 2018, pp. 1245–1249.

[65] D. Small, "Coordinated SAR acquisition planning for terrestrial snow monitoring," WMO, Washington, DC, USA, Tech. Rep. 0.9, 2014.

David Small (Senior Member, IEEE) received the B.A.Sc. degree in systems design engineering from the University of Waterloo, Waterloo, Canada, in 1988, the M.A.Sc. degree in electrical engineering from The University of British Columbia, Vancouver, Canada, in 1991, and the Ph.D. degree from the Remote Sensing Laboratories, Department of Geography, University of Zurich, Zurich, Switzerland, in 1998. His Ph.D. dissertation focused on the development of a processing chain for generating digital elevation models from repeat-pass ERS-1/2 data.

Since 2013, he has been leading the Environmental SAR Group, SARLab, Remote Sensing Laboratories, University of Zurich. In addition to geometric and radiometric calibration of synthetic aperture radar (SAR) imagery, he works on standardized approaches for terrain flattening to enable analysis ready data products. These are being demonstrated for a wide variety of applications, from SAR-based wet snow mapping in mountainous terrain, as well as applications in forestry and wide-area cryosphere mapping.

Christoph Rohner received the B.Sc. and M.Sc. degrees in geography from the University of Zurich, Zurich, Switzerland, in 2012 and 2014, respectively, where he is pursuing the Ph.D. degree with the Remote Sensing Laboratories.

In addition, since 2020 he has been working as part of the National Point of Contact (NPOC) for Satellite Images, Swiss Federal Office of Topography (swisstopo), Bern, Switzerland. His research interests include SAR time-series analysis of the cryosphere with a focus on glacier dynamics and wet snow cover estimation.

Nuno Miranda received the M.S. degree in telecommunications and signal processing from the University of Brest, Brest, France, in 1998.

He was with the University of Bordeaux III, Pessac, France, where he was involved in image processing. He was with the Center d"Études Spatiales de la BIOsphere, Toulouse, France, and the Centre National d'Études Spatiale (CNES) French Space Agency, Toulouse, where he was involved in SAR image segmentation and multitemporal filtering. In 2002, he joined European Space Agency (ESA), Paris, France, where he focused on the quality control and calibration of the ERS and ENVISAT (ASAR) Missions. In 2005, he teamed up with Altamira, Spain, on SAR interferometry. Since 2007, he has been with ESA, where he is responsible for the performance and algorithm of ESA's and Third Party SAR missions with the Sensor Performance, Product and Algorithm Section, Ground Segment and Mission Operations Department, ESA's Directorate of Earth Observation Programs.

Marius Rüetschi received the B.Sc. and M.Sc. degrees in geography from the University of Zurich, Zurich, Switzerland, in 2014 and 2017, respectively.

Since 2017, he has been part of the Remote Sensing Group, Land Change Science Unit, Swiss Federal Institute for Forest, Snow and Landscape Research WSL, Birmensdorf, Switzerland. His main research interest is the analysis of SAR time series of different land cover types with a special focus on forests and their dynamics.

Michael E. Schaepman (Senior Member, IEEE) received the M.Sc. and Ph.D. degrees in geography from the University of Zurich (UZH), Zurich, Switzerland, in 1993 and 1998, respectively.

In 1999, he was a Post-Doctoral Researcher with the Optical Sciences Center, University of Arizona, Tucson, AZ, USA. In 2000, he was appointed as a Project Manager of the European Space Agency APEX Spectrometer. In 2003, he became the Full Chair of Geoinformation Science and Remote Sensing, Wageningen University, Wageningen, The Netherlands. In 2009, he was appointed as the Full Chair of Remote Sensing with UZH, where he headed the Remote Sensing Laboratories, Department of Geography. In 2020, he became the President of UZH. His research interests include computational earth sciences using remote sensing and physical models, with a particular focus on using imaging spectroscopy for biodiversity mapping.